JOURNAL OF CATALYSIS 148, 113–118 (1994)

Iron–Aluminum Cluster Catalysts Obtained by Alkoxy Synthesis

1. Liquid-Phase Oxidation of Hexadecane

M. V. Tsodikov,*,[1] V. Ya. Kugel,* Yu. V. Maksimov,† O. G. Ellert,‡ V. M. Shcherbakov,‡ and O. V. Bukhtenko*

*Institute of Petrochemical Synthesis Russian Academy of Sciences, Leninsky pr., 29, Moscow 117912, Russia; †Institute of Chemical Physics, Russian Academy of Sciences, Kosygina ul., 4, Moscow 117977, Russia; and ‡Institute of General and Inorganic Chemistry, Russian Academy of Sciences, Leninsky pr., 31, Moscow 117912, Russia

Received April 8, 1992; revised October 18, 1993

Iron-substituted boehmite gel has been prepared by alkoxy synthesis, i.e., by reaction of $Fe(acac)_3$ with a fresh surface of AlOOH. Iron–aluminum complex oxide catalysts for liquid-phase oxidation of hexadecane were prepared by annealing the gel precursors. The gels with 0–20 wt.% of iron loading were studied by magnetic susceptibility and Mössbauer spectroscopy. Depending on the iron concentration, differing amounts of paramagnetic Fe^{3+} ions in the boehmite structure and small ferrimagnetic spinel clusters were observed in the X-ray amorphous precursors. Thermal treatment led to formation of substituted spinels, $Fe_xAl_{2-x}O_3$, as well as γ-ferric oxide clusters. The overall rate of hexadecane oxidation increased with an increase in the relative content of magnetic clusters. The inclusion of nonmagnetic Al^{3+} ions in the γ-Fe_2O_3 lattice reduced the number of terminal $Fe^{3+}{=}O$ groups and the overall catalytic activity. The role of electronically excited terminal oxygen on the surface of γ-ferric oxide clusters in the mechanism of hexadecane oxidation is discussed.

INTRODUCTION

Much attention has previously been devoted to simple metal oxides as catalysts for low-temperature liquid-phase oxidation of hydrocarbons (1–4). Although extensive studies have established their activity and selectivity, the mechanism of catalytic participation is far from clear. The majority of research work has revealed that the reaction itself seems to proceed in the liquid phase in accord with a radical-chain mechanism in which the catalyst surface is responsible for a radical initiation process that occurs either by hydroperoxide decomposition or by O_2, RH activation (2, 3). Indeed, oxygen activation, but not hydroperoxide decomposition, is assumed to be the initial step of cumene oxidation over Bi_2O_3 and ZnO catalysts (4).

[1] To whom correspondence should be addressed.

Despite the number of kinetic measurements (5–7) that have been carried out over simple metal oxides, data on catalyst structure and its relation with the reaction mechanism are still lacking. In particular, complex metal oxides and cluster catalysts have not been employed to explore this process.

This communication deals with iron–aluminum amorphous precursors and cluster catalysts prepared by alkoxy synthesis for liquid-phase oxidation of hexadecane. The goal of this work is to elucidate the relationship between the structure of the catalyst and the kinetic parameters of the process. Structural studies were carried out by magnetic susceptibility and Mössbauer spectroscopic methods.

METHODS

Iron-containing gels were prepared from a distilled benzene solution of aluminum isobutylate (or isopropylate) with iron acetylacetonate. $Fe(acac)_3$ was obtained electrochemically by anodic dissolution of iron in the acetylacetonate solution (8). The hydrolysis of aluminum alkoxide was carried out in 80% ethanol solution, which secured the formation of a pseudoboehmite aluminum hydroxide structure. The reaction of $Fe(acac)_3$ with the fresh surface of boehmite was accompanied by the decolorization of the solution. The gel formed was separated from the solution by centrifuging and then dried in air at room temperature and then under vacuum at 50°C. Iron concentration in the gel was varied by changing the $Fe(acac)_3/Al(OR)_3$ ratio in the starting benzene solution. The following gel precursors with different iron loadings were prepared: A (1–3 wt.% Fe), B (4–8) wt.% Fe), and C (12–25 wt.% Fe). The samples of iron–aluminum complex catalysts containing 2.5, 6.2, 13.6, and 20 wt.% Fe (samples II–V) were obtained by the subsequent annealing at 300°C (2 h) and 500°C (4 h) of the appropriate gels.

0021-9517/94 $6.00

For purposes of structural identification and kinetic evaluation, some model materials [γ-Al_2O_3 (I), γ-Fe_2O_3 (YII), and γ-Fe_2O_3 + 10% γ-Al_2O_3 (YI)] were prepared by precipitation, coprecipitation, and calcination at 400–450°C. The mean sizes of γ-Fe_2O_3 and γ-Fe_2O_3 + 10% γ-Al_2O_3, as estimated by X-ray analysis (URS-50 IM equipment with filtered Fe$K\alpha$ radiation), were ca. 6–7 nm.

Liquid-phase oxidation of hexadecane, both in the presence of metal oxide systems I–VII and in their absence ("blank" tests), was carried out in a closed, temperature-controlled, recirculating device at T + 160 ± 0.1°C and atmospheric pressure. The scheme of installation is given in Fig. 1. The reactor (1) was attached to a rocker whose back-and-forth motion produced the effective agitation of the liquid phase. Oxygen was circulated by means of a membrane compressor (3). The reaction products were removed by traps (5) containing SiO_2 and P_2O_5 adsorbents. Before a run, the system was evacuated and refilled with oxygen. The O_2 uptake was measured manometircally with a calibrated gas burette (6, 7). The overall reaction volume, hexadecane/oxygen ratio, and amount of powdered samples I–VII in each run were 6 cm^3, 1/10, and ca. 0.045 g, respectively. Special experiments showed that the oxidation rate was independent of the speed of the mixing.

S-like curves of O_2 uptake were similar for each catalyst. In the first stage of reaction the kinetic curve was described by the expression (9)

$$[O_2]_{abs} = W_{in}\tau + \Omega \cdot \sigma^2 \qquad [1]$$

where W_{in} is the initial oxidation rate, Ω is the autoacceleration factor, and τ is time. Using the second (quasi-linear) part of the overall kinetic curve, the maximum rate value (W_{max}) was obtained. Each of the kinetic parameters reported below was the mean value from at least three runs.

Structural studies were performed by Mössbauer spectroscopic and static magnetic susceptibility methods (10). Isomer shifts are reported relative to α-Fe. The spectra were computer-fit using the common minimization procedure for Mössbauer transition $\frac{3}{2} \rightarrow \frac{1}{2}$. The distribution of the internal magnetic fields (H_{in}) was analyzed using a modified program (11), which gives a direct estimate of hyperfine parameters (isomer shifts, quadrupole splittings, internal magnetic fields) through least-squares minimization.

Elemental analysis of the catalysts was carried out using a Perkin–Elmer AS-400 spectrometer. The values of specific surface area (S) were obtained by BET measurements with benzene as an absorbate (12).

RESULTS AND DISCUSSION

Gel Precursors

The temperature dependence of the static magnetic susceptibility, $\chi(T)$, is shown for $Fe(acac)_3$ and A–C gels in Fig. 2. As is seen, $\chi(T)$ for $Fe(acac)_3$ obeys the Curie law. The effective magnetic moment, μ_{eff}, calculated from the equation $\mu_{eff} = 2.828\sqrt{\chi_m T}$, where χ_m is the molar magnetic susceptibility corrected for molecular diamagnetism, is equal to 5.8 μ_B. This value is close to μ_{eff} = 5.92 μ_B typical of isolated Fe^{3+} (d^5) ions in an octahedral environment. In contast to $\chi(T)$ for $Fe(acac)_3$, $\chi(T)$ for gels A–C (Fig. 2, curves 1–4) obeys the Curie–Weiss law with a negative Weiss constant, θ. The increase in absolute values of θ from 10 to 150 K with increasing iron loading implies an increase in the antiferromagnetic exchange interaction between Fe^{3+} ions in the gel matrix.

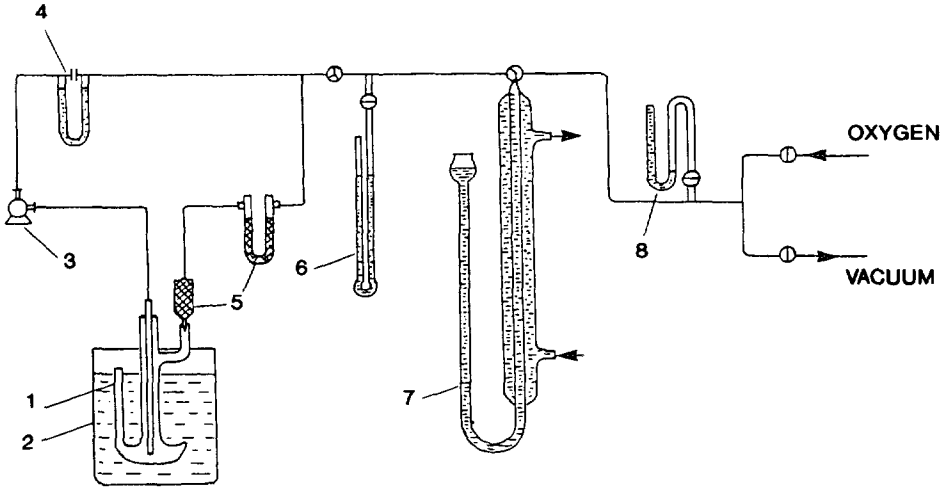

FIG. 1. Scheme of installation for low-temperature hexadecane oxidation. (1) Reactor; (2) thermostat; (3) circular pump; (4) gas flow meter; (5) traps for gas adsorption; (6) manometer; (7) gas burette; (8) vacuum gauge.

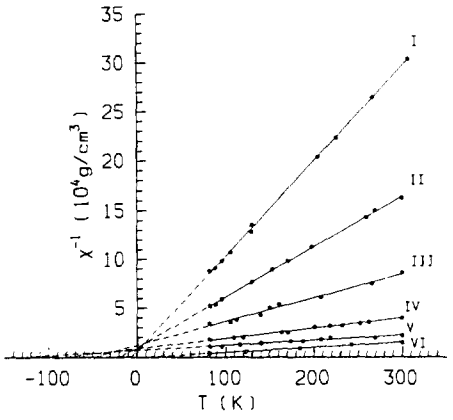

FIG. 2. Temperature dependence of inverse magnetic susceptibility. Iron in gels (wt.%): (I) 2.1; (II) 5.0; (III) 14.0; (IV) 20.0; (V) 25; (VI) $Fe(acac)_3$. *X* axis, temperature (K). *Y* axis, χ^{-1} (g/cm^3).

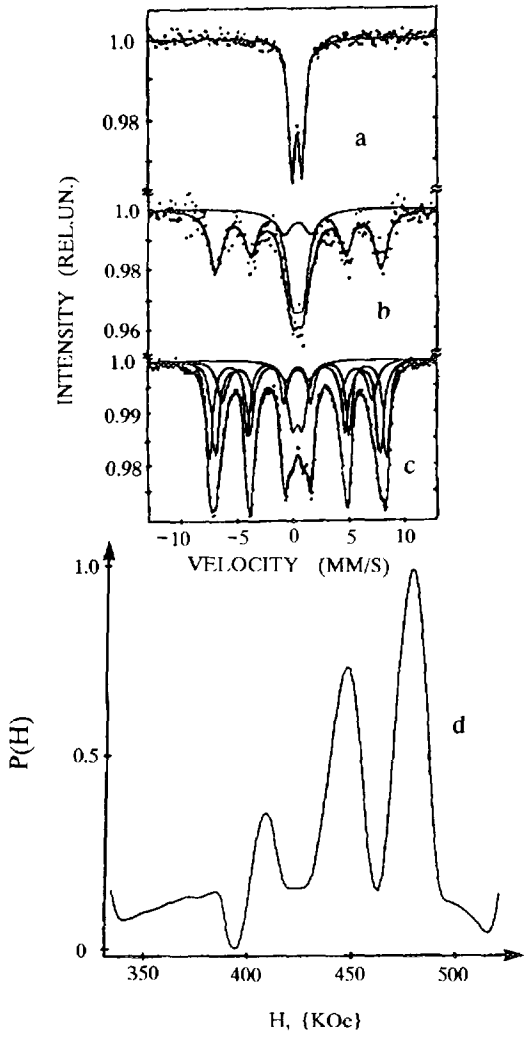

FIG. 3. Mössbauer spectra of gel C (14.0 wt.% Fe) (a–c) and field distribution function, $p(H)$, at 4.2 K (d). Temperatures (K): (a) 300; (b) 60; (c) 4.2. (a–c): *X* axis, mm/s. *Y* axis, intensity.

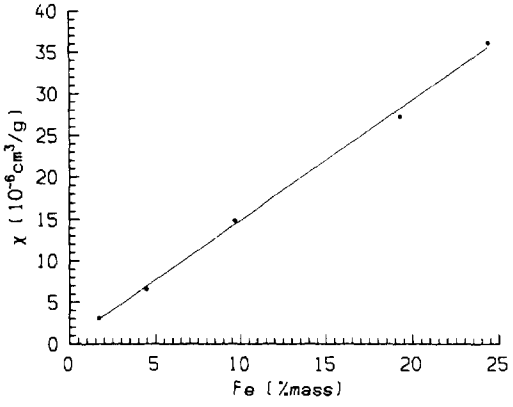

FIG. 4. Room-temperature dependence of magnetic susceptibility on iron loading. *X* axis, wt.% Fe. *Y* axis, magnetic susceptibility, χ (cm^3/g).

The typical room-temperature Mössbauer spectrum of gels A–C shows a doublet (Fig. 3a) of high-spin octahedrally coordinated Fe^{3+} (IS = 0.40 ± 0.03 mm/s, QS = 0.7 ± 0.08 mm/s) which significantly differs from the relaxation spectrum of $Fe(acac)_3$ (13).

Figure 4 shows the dependence of χ(300 K) on iron loading in the gels. The increase in χ(C) seems to indicate the presence of magnetic oxide clusters along with Fe^{3+} distributed in the "paramagnetic" boehmite matrix. In fact, the field dependence $\chi(H)$ for gel C shows nonlinearity even at 300 K, while for gels A and B it occurs at 77 K. Mössbauer data strongly support the presence of clusters. For example, the spectra of gel C (14 wt.% Fe) at T = 77–4.2 K (Figs. 3b–3d) are typical of an assembly of small superparamagnetic oxide clusters with a Curie point value $T_c \approx$ 25–30 K and two main maxima in the field distribution function, $p(H)$, with $H_{in} \approx 480 \pm 15$ kOe and $H_{in} \approx 450 \pm 20$ kOe (T = 4.2 K). For comparison, γ-Fe_2O_3 has two maxima at $H_{in} \approx 503 \pm 15$ kOe and $H_{in} \approx 460 \pm 15$ kOe. Upon transition from γ-Fe_2O_3 to γ-Fe_2O_3 + 10% Al_2O_3, H_{in} decreases by 10–20 kOe, while the Curie point drops from $T_c \approx 120$ K to $T_c \approx 60$ K. Since the average particle sizes of model samples are nearly the same ($\langle d \rangle \approx$ 6–7 nm), the H_{in} and T_c decrease is caused mainly by the substitution of iron by aluminum.

Thus, the genesis of iron-containing gels includes an interaction of $Fe(acac)_3$ with boehmite gel during which some weakening and bond rupture occur followed by an incorporation of Fe^{3+} ions into the boehmite matrix. Upon increased iron loading, an ever-increasing proportion of iron in spinel magnetic clusters takes place. Clusters like γ-Fe_2O_3 and γ-Fe_2O_3 + 10% Al_2O_3 possess spinel structures with mean particles not higher than $d \approx 5$ nm.

Kinetic and Structural Data

The kinetic curves of oxygen absorption in the presence of catalysts I–VII, as well as in the course of the "blank" reaction, are presented in Fig. 5. All sets of kinetic results

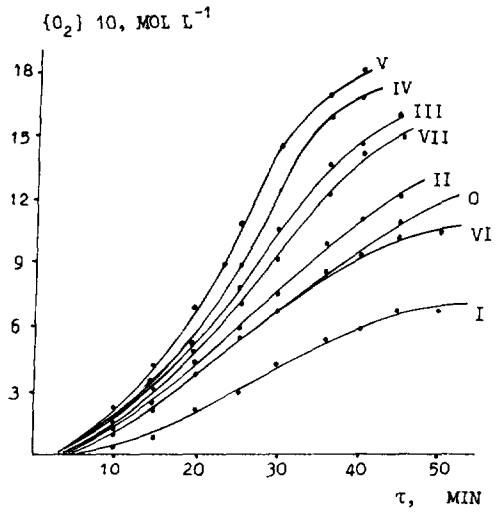

FIG. 5. Experimental kinetic oxidation curves for n-$C_{16}H_{34}$ over different oxides (T = 160°C, P = 0.1 MPa): (O) Without catalyst; (I) γ-Al_2O_3, iron loading, wt.%; (II) 2.5; (III) 6.2; (IY) 13.6; (V) 20.0; (VI) γ-Fe_2O_3 + 10% γ-Al_2O_3; (YII) γ-Fe_2O_3. X axis, time (min). Y axis, oxygen uptake (mol · L^{-1}).

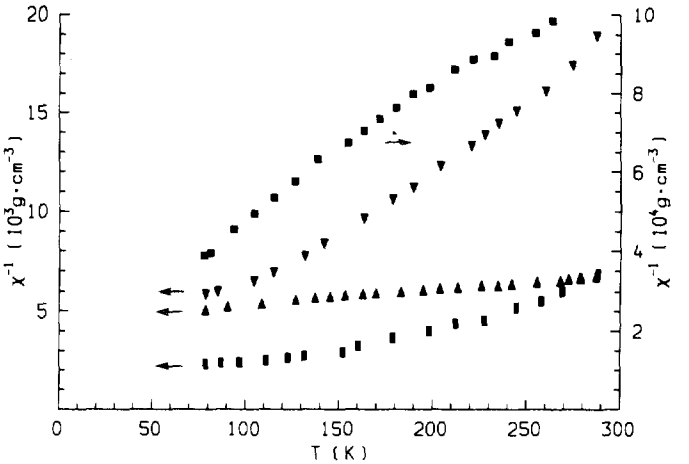

FIG. 6. Temperature dependence of the inverse magnetic susceptibility. (▮) Y; (■) III; (▼) YI; (▲) YII. X axis, temperature (K). Y axis, χ^{-1} (g/cm³).

are summarized in Table 1. The data show that compared to the "blank" reaction (0) each of the iron-containing oxides II–VII (except catalyst VI) promotes oxidation, while γ-Al_2O_3 inhibits the process. For samples II–V prepared by sol–gel technology, the indexes W_{max} and Ω increase with increased iron content, reaching maximum values at 20 wt.% Fe. It is also seen that the dilution of γ-Fe_2O_3 by aluminum (sample VI) leads to the loss of catalytic activity. It should be noted that in the row of iron-containing systems, sample VI may be considered a zero point whose catalytic ability is negligible; it is close to the uncatalyzed "blank" reaction.

Before the structural analysis it should be noted that all iron-containing catalysts obtained by alkoxy synthesis remained X-ray amorphous after thermal treatment. The presence of a halo typical of γ-Al_2O_3 suggests that amorphous spinel is the basic structure of created catalytic systems.

Analysis of the temperature dependence of static magnetic susceptibility (Fig. 6) shows that practically all of catalysts II–VII are magnetically inhomogeneous. In fact, on the basis of $\chi(H)$ dependence at different temperature (Figs. 7 and 8) one can deduce the existence of magnetically ordered clusters in samples II–V, which is strongly supported by Mössbauer spectroscopic data.

Figure 9 presents the typical Mössbauer spectra of sample V before annealing (boehmite form a) and after thermal treatment taken at T = 300–4.2 K (b–d). As one can see, the annealing noticeably changes the structure of the catalyst. First, the quadrupole splitting of the Fe^{3+} high-spin complex increases essentially in the annealed form

TABLE 1

Specific Surface Area (S_{sp}) and Kinetic Parameters of Hexadecane Oxidation over Catalysts I–VII

N	Catalyst	Iron content (wt.%)	S_{sp} (m^2/g)	Maximum rate ($W_{max} \times 10^4$ mol/liter · s)	Factor of autoacc ($\Omega \times 10^6$ mol/liter · s^2)
O	No catal.	0	—	4.7	0.220
I	γ-Al_2O_3	0	305	3.3	0.180
II	$Fe_xAl_{2-x}O_3$	2.5	296	6.0	0.220
III	$Fe_xAl_{2-x}O_3$	6.2	290	8.4	0.250
IV	$Fe_xAl_{2-x}O_3$	13.6	290	11.2	0.310
V	$Fe_xAl_{2-x}O_3$	20.0	285	13.0	0.430
VI	γ-Fe_2O_3+ 10% γ-AL_2O_3	63	140	4.8	0.225
VII	γ-Fe_2O_3	70	190	8.9	0.270

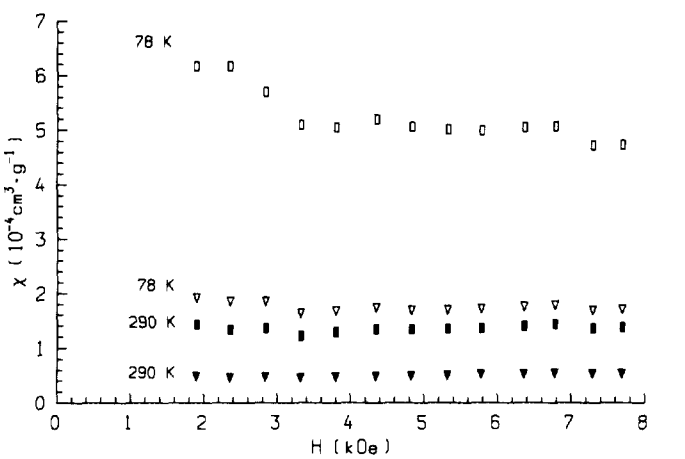

FIG. 7. The magnetic susceptibility vs external magnetic field. (▮) 300 K; (□) 77 K (catalyst Y); (▼) 300 K, (▽) 77 K (catalyst YI). X axis, external field, H (kOe). Y axis, magnetic susceptibility, χ (cm^3/g).

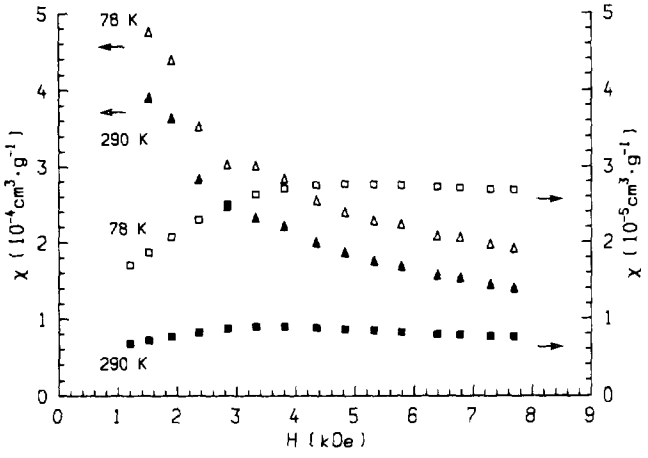

FIG. 8. The magnetic susceptibility vs external magnetic field. (▲) 300 K; (△) 77 K (catalyst YII); (■) 300 K; (□) 77 K (catalyst III). X axis, external field, H (kOe). Y axis, magnetic susceptibility, χ (cm^3/g).

compared to iron-containing gel (QS = 1.22 ± 0.05 mm/s against QS = 0.75 ± 0.05 mm/s, respectively). The significant axial distortion of local polyhedron FeO_6 in the substituted spinel $Fe_xAl_{2-x}O_3$ seems to be caused by the small size and disorder in layer stacking of the γ-alumina. Second, the annealing leads to cluster formation. In fact, two patterns of hyperfine structure lines with $H(1)_{in} \approx$ 495 kOe and $H(2)_{in} \approx$ 460 kOe from magnetite clusters are clearly seen even at room temperature (Fig. 9b). At T = 4.2 K about 45% of total spectral area is the set of hyperfine structure (HFS) patterns corresponding to magnetic clusters. The largest value of $H_{in} \approx$ 520 kOe is very close to that typical of large particles of γ-ferric oxide (14). A considerable part of the resonance absorption (≈ 45%) shown by the wide monoline appears to belong to small clusters magnetically unstable even at T = 4.2 K.

The correlation between catalytic activity and low-temperature Mössbauer data on the relative content of magnetic clusters in the samples is presented in Fig. 10. The total amount of iron in clusters was evaluated from the spectral area under HFS lines at 4.2 K. The overall activity of complex oxide catalyst is directly proportional to the relative cluster content.

Model of Active Surface

Magnetic clusters in samples II–Y belong to a class of inverse spinels. Any intermediates between magnetite (Fe_3O_4) and maghemite (γ-Fe_2O_3) can be easily obtained by the low-temperature oxidation of magnetite according to the quasichemical equation (15)

$$Fe_A^{3+}[Fe^{2+}Fe^{3+}]_BO_4^{2-} \rightarrow Fe_A^{3+}[(Fe^{2+}_{1-3\delta}Fe^{3+}_{1-3\delta})Fe^{3+}_{5\delta}V_\delta]_BO^{2-}, \quad [2]$$

where A and B are tetrahedral and octahedral sublattices, V is cation vacancy, $(Fe^{2+}_{1-3\delta}Fe^{3+}_{1-3\delta})$ are cations participat-

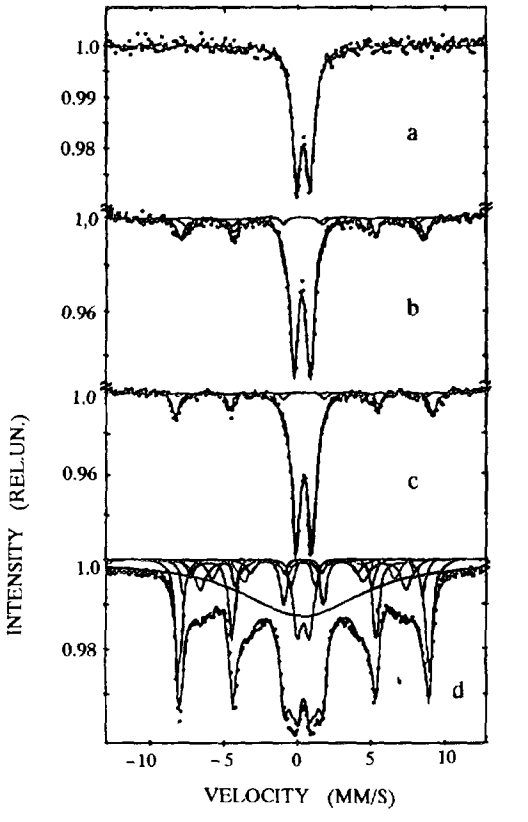

FIG. 9. Mössbauer spectra of catalyst Y, taken at 300–4.2 K: (a) initial gel (300 K); (b–d) the same after calcination: (b) 300 K, (c) 80 K, (d) 4.2 K. X axis, velocity (mm/s). Y axis, intensity (arb. units).

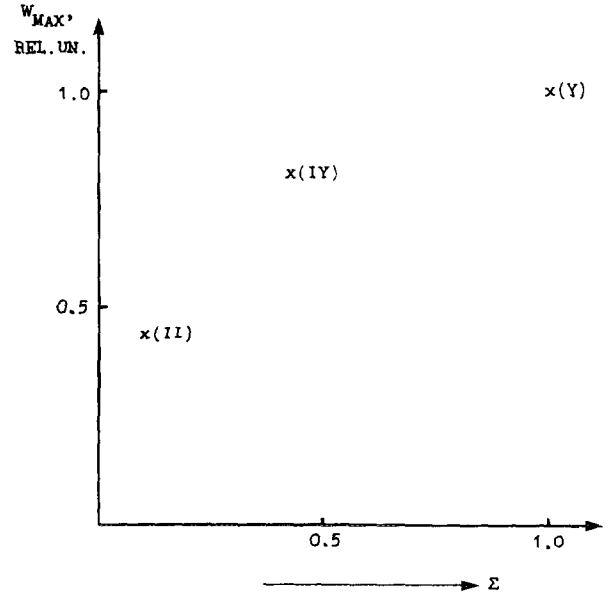

FIG. 10. Correlation between maximum oxidation rate (W_{max}) and relative magnetic cluster content (Σ). X axis, relative magnetic cluster content (Σ). Y axis, W_{max} (rel. un.).

ing in Verwey double electron exchange, and δ is a parameter of nonstoichiometry changing values between 0 and $\frac{1}{3}$ upon transition from Fe_3O_4 to γ-Fe_2O_3.

It is seen from Eq. [2] that each cation vacancy removes five Fe^{3+} cations from the "paired" Verwey exchange, forming terminal $Fe^{3+} = O^{2-}$ groups. By analogy with the properties of vanadyl, chromyl, and molybdenyl groups, one may suggest that the surface oxygen of the γ-ferric oxide cluster acquires the anion-radical behavior due to thermal electron–phonon excitation accompanied by the shift in the electron density from O^{2-} to Fe^{3+} (16, 17). The indirect proof for this comes from the luminescence and radiothermoluminescence data (18, 19) according to which a high probability for radiationless transitions in octahedral complexes of *d*-metal oxides may result from thermal excitation because of the intersection of potential curves for ground and lowest excited states. The anion radical, formed upon lattice oxygen excitation, may partake in anion-radical reactions and, in particular, in free radical generation via breakage of R–H bonds accompanied by the hydroxylation of the surface (17).

The substitution of magnetic Fe^{3+} by nonmagnetic Al^{3+} upon transition from γ-Fe_2O_3 (sample YII) to γ-Fe_2O_3 + 10% Al_2O_3 (sample YI) considerably changes the electronic character of the terminal $Me = O$ bond and diminishes the absolute number of the active centers. In fact, it seems to take more energy to excite the $Al^{3+} = O$ terminal group than the $Fe^{3+} = O$ bond. The corresponding decrease in overall activity (Table 1) clearly shows the structural and surface sensitivity of the reaction of hexadecane liquid-phase oxidation.

Let us estimate, in conclusion, the gain in overall activity of the best complex catalyst V compared to that of simple oxide VII. By taking into account the data from elemental analysis, Mössbauer spectroscopy, and magnetic measurements, the total surface area of magnetic clusters in catalyst Y is roughly $S(Y) \approx 20$–$30\ m^2/g$. Thus, the normalized activity (per surface unit) of complex oxide Y is more than an order of magnitude higher than that of catalyst YII. On the other hand, the inclusion of nonmagnetic Al^{3+} ions in the lattice of oxide catalyst VII reduces the surface concentration of terminal $Fe^{3+} = O$ groups and decreases values of exchange integrals and effective sublattice moments. As a result, the catalytic ability drops remarkably (Table 1).

REFERENCES

1. Margolis, L. Ya., "Okyslenia Uglevodorodov na Geterogennych Katalysatorach," p. 327. Chimia, Moscva, 1977.
2. Golodetch, G. E., "Geterogenno-Katalyticheskoe Okyslenie Organicheskicn Veshestv," p. 375. Naukova dumka, Kiev, 1978.
3. Gorochavatsky, Ya. V., Kotnienko, T. P., and Shalya, V. V., "Geterogennogomogennye Reakcii," p. 204. Technica, Kiev, 1972.
4. Emanuel, N. M. (Ed.), "Teoria i Practica Gidkophaznogo Okyslenia," p. 330. Nauka, Moskva, 1974.
5. Emanuel, N.M., *Petrochemia* **18**(4), 485 (1978).
6. Norikov, Yu. D., Bogorishvilli, M. K., Salivadze, L. V., and Blumberg, E. A., *in* "Theory and Practice of Liquid Phase Oxidation" (N. N. Emanuel, Ed.), p. 193. Nauka, Moscow, 1974.
7. Rubinskaya, O. P., Kuzmina, G. N., and Sanin, P. I., *Petrochemia* **22**(5), 661 (1982).
8. Shreider, V. A., Turevskaya, E. P., Kozlova, N. I., and Turova, N. Ya., *Inorg. Chim. Acta* **53**, L73 (1981).
9. Mazolezkii, A. B., Vinogradova, V. G., and Panova, G. V., *Petrochemia* **27**(6), 796 (1987).
10. Maksimov, Yu. V., Matveev, V. V., Suzdalev, I. P., Tsodikov, M. V., and Ellert, O. G., *Hyperfine Interact.* **56**, 1983 (1990).
11. Wivel, C., and Morup, S., *J. Phys. E* **14**(5), 605 (1981).
12. Brunauer, S., Deming, L. S., Deming, W. E., and Teller, E., *J. Am. Chem. Soc.* **62**, 1723 (1940).
13. Tsodikov, M. V., Ivanova, G. F., Bukhtenko, O. V., Ellert, O. G., Maksimov, Yu. V., and Zaslavskii, B. A., *Bull. Acad. Sci. USSR, Div. Chem. Sci.* (Engl. Transl.) **8**, 1898 (1988).
14. Berkowitz, A. E., Lahut, J. A., Jacobs, I. S., and Levinson, L. M., *Phys. Rev. Lett.* **34**, 595 (1975).
15. Morozova, O. S., Maksimov, Yu. V., Shashkin, D. P., Shirjaev, P. A., Zhorin, V. A., and Krylov, O. V., *Appl. Catal.* **78**, 227 (1991).
16. Gritscov, A. H., Shvets, V. A., and Kazansky, V. B., *Chem. Phys. Lett.* **35**(4), 511 (1975).
17. Kazansky, V. B., in "Proceedings, 6th International Congress on Catalysis, London, 1976" (G. C. Bond, P. B. Wells, and F. C. Tompkins, Eds.), Vol. 1, p. 50. The Chemical Society, London, 1977.
18. Kazansky, V. B., Pershin, A. N., and Shelimov, B. N., *in* "Proceedings, 7th International Congress on Catalysis, Tokyo 1980" (T. Seiyama and K. Tanabe, Eds.), Vol. 1, p. 1210. Elsevier, Amsterdam, 1981.
19. Maksimov, Yu. V., and Gustov, V. V., *Chimia Vysokich Energii* **14**(6), 505 (1980).